Water Practice & Technology

IWA PUBLISHING

Water Practice & Technology Vol 18 No 5, 1099 doi: 10.2166/wpt.2023.069

Electrocoagulation process for the decolorization of wastewater containing Reactive Red 195 and CFD simulation of the hydrodynamic in a continuous-flow single-channel reactor

Raowia Lamhar[a,*], Toussaint Ntambwe Kambuyi[b], Zakia Zmirli[c], Anas Aguelmous[c], Bouchra Bejjany[a], Khalid Digua[a] and Adil Dani[a]

[a] Laboratory of Process and Environmental Engineering, Faculty of Sciences and Technics of Mohammedia, Hassan II University of Casablanca, Mohammedia, Morocco
[b] Laboratory of Chemical Engineering, UMR CNRS 5503, Campus University of Toulouse III-Paul Sabatier, FSI. 118, Narbonne road, Toulouse 31062, France
[c] Laboratory of Advanced Materials and Process Engineering, Faculty of Sciences, Ibn Tofail University, Kenitra, Morocco
*Corresponding author. E-mail: raowia.lamhar@gmail.com

ABSTRACT

The highly colored textile effluents require efficient treatment before being released into the environment. In this study, a continuous-flow single-channel reactor operating in closed- circuit was used to apply electrocoagulation for the treatment of synthetic textile wastewater. First, the characterization of the hydrodynamic within the reactor is evaluated by Computational Fluid Dynamics simulation using the k-ε turbulence model (Comsol Multiphysics®). Apart from a non-uniform distribution of the velocities inside the reactor, no particular anomaly was observed. Second, the decolorization efficiency was examined under various current intensities, electrolysis times, and initial dye concentrations. By operating under a current intensity of 100 mA instead of 50 mA, the required electrolysis time to achieve a decolorization efficiency of 80% decreased by 40%, while the specific electrode consumption remained slightly unchanged at about 0.19 kg Al·kg^{-1}. At a current intensity of 100 mA and an electrolysis time of 26 min, and the increase in the initial dye concentration from 10 to 50 mg·L^{-1} the decolorization efficiency decreased remarkably while the specific electrode consumption was kept constant at about 0.15 kg Al·kg^{-1} dye removed. The knowledge obtained through this study can be used for the transposition from batch to continuous mode.

Key words: CFD simulation, CFSC reactor, decolorization, electrocoagulation, RR195, textile wastewater

HIGHLIGHTS

- The EC process was carried out in a recirculation mode.
- Comsol Multiphysics was used to perform CFD simulation in order to investigate the transport phenomenon in the CFSC reactor.
- The RTD study is used to validate the numerical results obtained by CFD simulation.
- The current intensities applied are far lower than in a conventional EC cell.
- 0.15 kg/kg was considered to be the limit value of the specific electrode consumption.

GRAPHICAL ABSTRACT

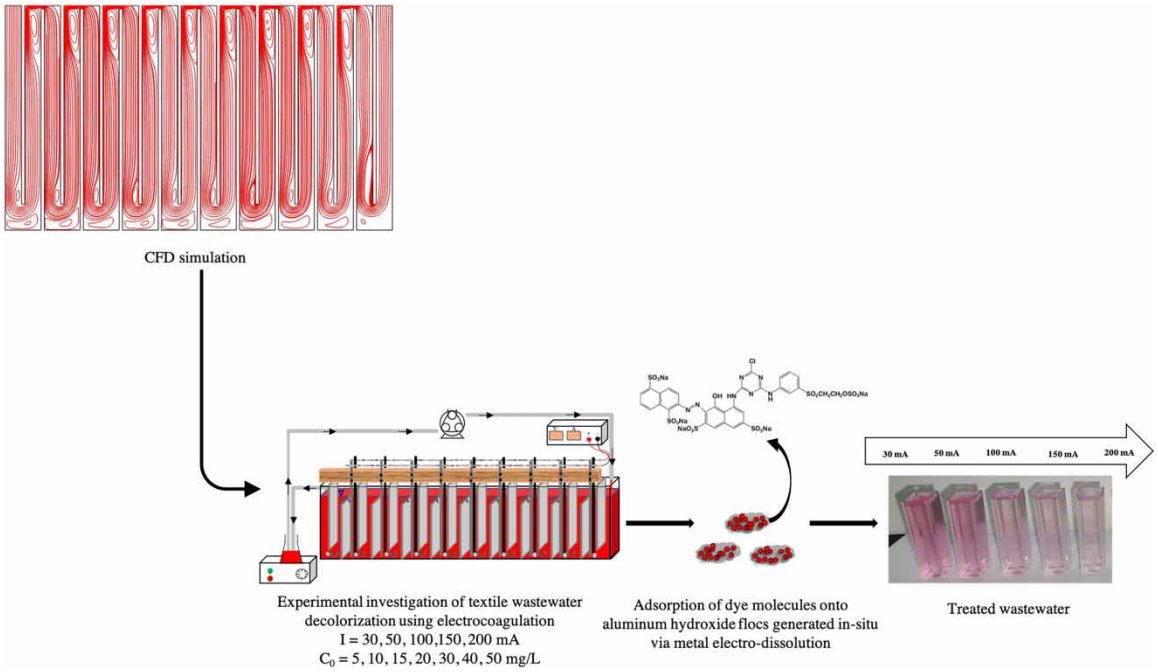

1. INTRODUCTION

Textile industries are known to be among the most water-consuming and polluting industries (Samanta *et al.* 2019), the World Bank indicates that 17–20% of industrial wastewater comes from textile wet processing (Zheng *et al.* 2022). The latter generates effluents containing acids, alkalis, dyes, print pigments, hydrogen peroxide, starch, soaps, metals, and surfactants, to name a few (Bidu *et al.* 2021). Depending on the dye composition and the dying process, 10–50% of the dye initial amount is released in the discharged effluents (Ammayappan *et al.* 2016), with such a complex composition, constituting thus a major environmental issue. Moreover, reactive dyes are among the most problematic for the environment due to their bright colors, high solubility in water, and low fixation degree (50–90%). Numerous techniques were previously used to remove Reactive Red 195 (RR195) from synthetic wastewater, namely adsorption (Dey & Kumar 2017; Pérez-Calderón *et al.* 2018; Gündüz & Atabey 2019; Mahanna & Samy 2020; Munagapati *et al.* 2022), sonoelectrochemical oxidation (Somayajula *et al.* 2012), chemical coagulation (Thammachai & Charoensuk 2021), electrochemical oxidation process (Umadevi *et al.* 2022), electro-Fenton (Nazari & Setayesh 2019), and electrocoagulation (EC) (Criado *et al.* 2020). Compared to the other processes, the EC process guarantees multiple desired outcomes such as chemical dosage reduction and sludge generation reduction (Moussa *et al.* 2017; Tegladza *et al.* 2021), and, unlike most conventional processes, the EC process provides *in situ* delivery and compact equipment (Criado *et al.* 2020). EC is a wastewater remediation method that has been broadly studied for the decolorization of wastewater containing RR195 and for the removal of a large range of contaminants such as: heavy metals (Doggaz *et al.* 2019), suspended solids (Ntambwe Kambuyi *et al.* 2019), oils (Yang *et al.* 2021), dyes (Criado *et al.* 2020), Fluorides (Graça *et al.* 2019). The EC process involves the electrochemical dissolution of the sacrificial metal leading to the release of metal ions, which undergo hydrolysis reactions forming various metallic hydroxides precipitates (coagulants). Simultaneously, at the cathode, electrolytic hydrogen gas bubbles are generated. These bubbles allow a solid–liquid separation via flotation of the coagulated particles (flocs).

The design of the EC process, mainly the operation mode and the reactor geometry, strongly affects its operation and efficiency. The majority of published studies on wastewater treatment using the EC process are characterized by the use of small reactors (volume ranging from 100 mL to 1 L) operating in batch mode. According to Garcia-Segura *et al.* (2017), most experimental works lean toward stirred batch cells with plate electrodes rather than other reactor geometries that can provide higher efficiency and lower energy consumption. In the last decades, much effort has been put into the design and application of continuous-flow EC reactors in the wastewater treatment and decolorization (Amour *et al.* 2016; Benazzi *et al.* 2016). In this context, Ardhan *et al.* (2015)

published an interesting paper based on the design of a continuous-flow reactor using experimental batch data for the decolorization of Reactive Blue 21 by EC. The steady-state conditions could often be predicted using experimental data from the reactor operating in batch mode (Bennajah *et al.* 2009; Attour *et al.* 2014; Rodrigues *et al.* 2020). However, the continuous-flow operation mode leads to flow malfunctions that can reduce the contact time between the coagulants and the pollutants, resulting in low treatment or decolorization efficiency. As such, the total or partial recycling of the solution leaving the reactor may be an interesting outcome as it allows the reuse of the coagulant leaving the reactor.

Additionally, the geometry of the reactor has great influence on bubble path, solid–liquid separation (flotation/settling), floc formation, fluid flow regime, and mixing characteristics (Hakizimana *et al.* 2017). Hence, for a given reactor geometry, the characteristics of the hydrodynamic as well as their influence on the mechanisms that occur within the reactor must be considered when investigating the reactor performance. Computational Fluid Dynamics (CFD) has been used to assess various aspects of flow through electrochemical reactors (Choudhary & Mathur 2017; McBeath *et al.* 2020; Villalobos-Lara *et al.* 2020).

This work investigates the decolorization of Reactive Red 195 using the EC process in a continuous-flow single-channel (CFSC) reactor operating in closed-circuit. The configuration allows a total recycling of the solution at the outlet of the reactor. The performance of the system is evaluated as a function of transfer and transport phenomena that govern the process. This paper is outlined as follows: first, the characterization of the hydrodynamic within the CFSC reactor is performed by CFD simulation using Comsol Multiphysics®. An experimental Residence Time Distribution (RTD) study is then used to validate the numerical results obtained by CFD simulation. Second, the experimental study of the decolorization of the wastewater containing RR195 is investigated as a function of various parameters such as initial dye concentration, applied current intensity, and electrolysis time.

2. MATERIALS AND METHODS

2.1. Synthetic wastewater preparation

The experiments were carried out using Reactive Red 195 (RR195) supplied by Meghmani Dyes and Intermediates LLP. Table 1 shows the properties of the RR195 including its chemical class, molecular weight, maximum absorption wavelength, and chemical structure. The textile dye was used without any further purification in order to represent real dyeing conditions.

Table 1 | Properties of the Reactive Red 195 (RR195)

Dye	Chemical structure	M_w (g · mol^{-1})	Chemical class	λ_{max} (nm)
Reactive Red 195	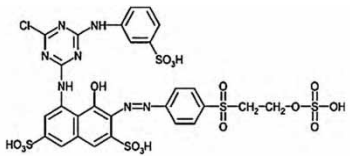	1,136.3	Monoazo	542

The preparation of synthetic wastewater consisted of mixing the RR195 with distilled water using a magnetic stirrer. The initial concentration was varied between 5 and 50 mg · L^{-1}, while the initial conductivity was set at 2, 400 μS · cm^{-1} used in previous studies (Merzouk *et al.* 2009) and adjusted using sodium chloride (NaCl) which is the most essential auxiliary added in the reactive dyeing of many cellulosic fibers to enhance dyes' exhaustion (Burkinshaw & Salihu 2018). The initial pH was maintained at 7 as the EC removal efficiency is proven to be the most efficient between 5 and 9. At this pH range, the prevailing species are $Al(OH)_3$ which are characterized by their large specific surface area (Aoudj *et al.* 2010).

2.2. Experimental apparatus

Figure 1 shows the experimental apparatus which consisted of a key part and a utility part. The key part included operations that directly affect the treatment such as the CFSC reactor with the electrical components (electrodes and power supply) and the storage tank that allowed us to harvest samples. The utility part included the needed

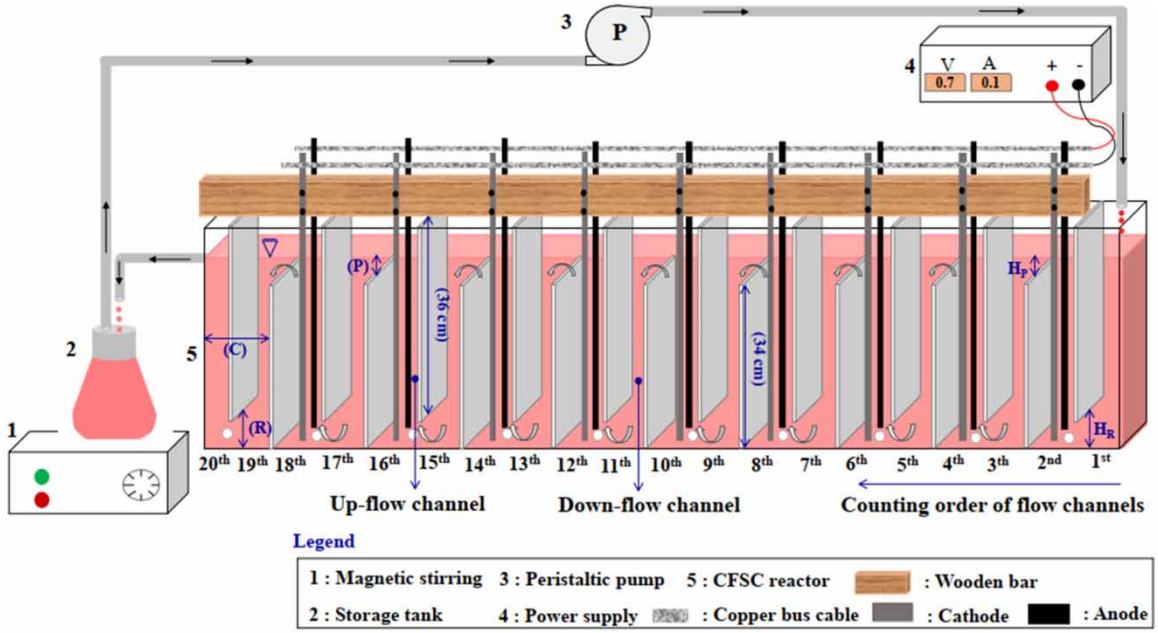

Figure 1 | Schematic representation of the CFSC reactor operating in a closed-circuit.

services that are necessary to the success of the key operations but do not involve any changes in the solution treatment such as: magnetic stirrer, peristaltic pump, piping system, and copper bus cable.

The entire closed-circuit consisted of a volume of 9.445 L, 5% of which constituted the storage tank volume. This configuration allowed recycling 100% of the treated solution along with the flocs.

The CFSC reactor (40 cm high, 59.5 cm long, and 5 cm wide) used in this study was previously designed and used by Ntambwe Kambuyi *et al.* (2021). It is made of transparent glass and is split into 10 rectangular compartments arranged in series. Each compartment (C), with a width of 5 cm, is divided equally into two channels: upflow and downflow channels connected to each other through a passage zone (P) with a height (H_P) of 0.5 cm and recirculation zone (R) with a height (H_R) of 4 cm. The liquid height inside the CFSC reactor while functioning is 34.5 cm. H_P of 0.5 cm allows a maximum flow velocity in the vicinity of the free surface leading to flocs entrainment resulting in a high coagulant specific surface area, while H_R of 4 cm enables flocs settling at the bottom of the CFSC reactor. This configuration allows a vertical serpentine flow, which improves mixing within the reactor. Since the cross-section is different in the flow channels, the passage, and the recirculation zone, the flow velocity is not uniformly distributed throughout the volume of the CFSC reactor for a given volumetric flowrate.

Aluminum electrodes plates (of 50 cm height, 2 cm width, and 0.2 cm thickness) arranged in a monopolar-parallel configuration were used as anodes and cathodes. The experiments were conducted under galvanostatic mode; different current intensities were applied to nine pairs of electrodes placed in the first nine upflow channels (one pair per upflow channel) as shown in Figure 1. A copper bus cable and a wooden bar were used, respectively, to connect the anodes (as well as the cathodes) to each other and to fix an inter-electrode distance (d_{int}) of 14 mm. The total active electrode surface S_a was equal to 621 cm^2 (34.5 cm $\times$ 2 cm is the surface of each electrode), and the corresponding S_a/V_T ratio for the entire closed-circuit was equal to 6.57 $m^2 \cdot m^{-3}$. A high active electrode surface was chosen in order to avoid the increase in energy consumption. The electrodes were initially rubbed with sandpaper to remove the passive oxide layer, rinsed with tap water, and immersed into diluted acetone to eliminate dye traces from former tests. Finally, they were dipped in 3-M HCl solution to prevent possible electrode passivation. The electrodes were rinsed with distilled water and dried for use.

2.3. Analytical methods

The conductivity was measured using the portable conductor HI 99300 of HANNA brand. The resolution of the conductivity meter is 1 $\mu S \cdot cm^{-1}$ and the measurement ranges from 0 to 3, 999 $\mu S \cdot cm^{-1}$ with an accuracy of $\pm$2% full scale. Samples were periodically taken at the outlet of the reactor after treatment, centrifuged at

4,000 rpm for 2 min using Hettich ROTOFIX 32A centrifuge. The absorbance was measured before and after treatment using UV-visible spectrophotometer HITACHI, U5100 model at a maximum wavelength of 542 nm.

The decolorization efficiency (η) was determined to evaluate the treatment of synthetic wastewater containing RR195 in laboratory-scale EC process:

$$\eta\ (\%) = \frac{C_0 - C_t}{C_0} \times 100 \tag{1}$$

where C_0 and C_t represent the initial and the dye concentration at a determined time t ($\text{mg} \cdot \text{L}^{-1}$), respectively. The corresponding dye concentration value was determined using a calibration curve.

The amount of electro-dissolved aluminum (m_{th}) was calculated using Faraday's law as follows:

$$m_{th}(\text{g} \times \text{m}^{-3}) = \frac{3,600 \times M \times I \times t}{z \times F \times V_T} \tag{2}$$

where M is the molecular weight of aluminum ($26.8\ \text{g} \cdot \text{mol}^{-1}$), z is the number of electrons corresponding to aluminum oxidation ($z = 3$), F is the Faraday's constant ($96,500\ \text{C} \cdot \text{mol}^{-1}$), V_T is the total volume of the treated synthetic wastewater (m^3), I is the current intensity (A), and t is treatment time (h).

Given the neutral pH, the dissolution of aluminum is exclusively electrochemical (Cañizares *et al.* 2005). The specific electrode consumption denoted as μ_{Al} ($\text{kg Al} \cdot \text{kg}^{-1}$ dye removed), is defined as the ratio of the amount of electro-dissolved aluminum and the amount of dye removed from the solution. It can be expressed as follows:

$$\mu_{Al}(t) = \frac{m_{th}(t)}{(C_0 - C_t)} \tag{3}$$

2.4. RTD experiment

The mixing flow pattern inside the CFSC reactor was obtained using the RTD method. The experimental distribution function obtained was used to validate the results of the numerical simulation performed through CFD. In order to maintain a constant residence time, the inlet flowrate was adjusted to $84.5\ \text{L} \cdot \text{h}^{-1}$. The stimulus–response technique based on pulse injection was employed using $3\ \text{mol} \cdot \text{L}^{-1}$ of potassium chloride as a tracer. A volume of 1 mL of the tracer was injected during 4 s. The RTD experiments were performed without the electrodes in order to prevent possible solution conductivity variations. The conductivity of the outlet liquid samples was measured for hydrodynamic analysis using the distribution function $F(t)$.

2.5. CFD simulation

To perform the CFD simulation of the CFSC reactor, COMSOL Multiphysics® was used and some assumptions related to the operating conditions were defined. First, the flow was assumed to be incompressible and due to the complete dilution of dye in water, the chemical and physical properties of the solution were considered to be similar to those of water (especially the density and dynamic viscosity). Moreover, the CFD simulation was performed without electrodes inside the reactor, assuming that electrochemical reactions do not significantly affect the hydrodynamic behavior within the reactor. Therefore, globally, the hydrodynamic in the reactor is controlled by the liquid flowrate.

The CFD simulation was performed by coupling the single-phase Reynolds Averaged Navier–Stokes (RANS) equations with low-Reynolds-number k–ε turbulence model (Equations (4)–(6)) and the convection-diffusion equation (Equation (10)). The RANS equations with Reynolds-number k–ε turbulence model were solved to study the hydrodynamics inside the CFSC reactor in order to describe the flow velocity profile in different parts of the reactor. The low-Reynolds-number k–ε turbulence model was preferred in this study because it provides a very accurate description of the boundary layer compared to the standard k–ε model (Nie & Li 2015).

$$\rho(u \cdot \nabla)u = \nabla \cdot \left[-\rho I + (\mu + \mu_T)(\nabla u + (\nabla u)^T) - \frac{2}{3}(\mu + \mu_T)(\nabla \cdot u)I - \frac{2}{3}\rho k I\right] + F \tag{4}$$

$$\nabla \cdot u = 0 \tag{5}$$

$$\rho(u \cdot \nabla \mathrm{k})^{\cdot} = \nabla \cdot \left(\left(\mu + \frac{\mu_T}{\sigma_k} \right) \nabla \mathrm{k} \right) + P_k - \rho\varepsilon \tag{6}$$

$$\rho(u \cdot \nabla)\varepsilon = \nabla \cdot \left[\left(\mu + \frac{\mu_T}{\sigma_\varepsilon} \right) \nabla \varepsilon \right] + C_{e1} \frac{\varepsilon}{k} P_k - C_{e2} \rho \frac{\varepsilon^2}{k} \tag{7}$$

Turbulent viscosity equation reads as:

$$\mu_T = \rho C_\mu \frac{k^2}{\varepsilon} \tag{8}$$

The production term is expressed as:

$$P_k = \mu_T \left[\nabla u : (\nabla u + (\nabla u)^T) - \frac{2}{3} (\nabla u)^2 \right] - \frac{2}{3} \rho k \nabla \cdot u \tag{9}$$

$$\frac{\partial C}{\partial t} + \nabla \cdot (-D \nabla \cdot C) = R - u \cdot \nabla C \tag{10}$$

where C is the tracer concentration, $D = D_{mol} + D_{turb}$ is the total diffusion coefficient, D_{mol} is the coefficient of molecular diffusion, D_{turb} is the coefficient of turbulent diffusion, R is the reaction rate ($R = 0$ because the tracer must be inert), and u is the velocity. The turbulent diffusivity D_{turb} was considered equal to the turbulent kinematic viscosity.

As for boundary conditions, a constant normal velocity boundary condition was applied at the inlet of the CFSC reactor ($u = -u_0$). The turbulent intensity and the turbulent length scale were equal to 0.05 (5%) and 0.025 m, respectively. At the outlet of the CFSC reactor, the boundary condition was set to zero ($p = 0$). The zero-shear boundary condition was applied to the surface of the upper part (free surface) of the reactor. The no-slip boundary condition was applied for the remaining boundary of the CFSC reactor (the surface of the lower part, the surface of baffles, etc.). Considering the vertical serpentine flow in our case, the force of gravity was taken into account.

The convection–diffusion (Equation (10)) was solved to obtain a numerical result, which was compared to the experimental one for validating the results obtained by CFD.

A constant concentration of the tracer boundary condition was applied at the inlet of the CFSC reactor. For the outlet, the zero diffusive flux boundary condition was applied, which implies that the mass flux was purely convective. Also, the zero-flux boundary condition was applied at the free surface and at the remaining parts of the CFSC reactor.

3. RESULTS AND DISCUSSION

3.1. CFD simulation of the hydrodynamic

The CFD simulation is performed using a boundary layer mesh for the discretization of domains. This type of mesh is typically used for fluid flow problems to resolve the thin boundary layers along the no-slip boundaries. First, the solution of the hydrodynamics was evaluated for different mesh numbers until the numerical average velocity was approximately equal to the analytical one calculated using Q/S (Q is the flowrate equal to 84.5 $\mathrm{L \cdot h^{-1}}$ and S is the area across of the flow channel that is equal to 12.5 $\mathrm{cm^2}$). The comparisons are made for the upflow channel 11 and the downflow channel 12 at $y = 0.17$ m. The results show that the relative error ε values between numerical and analytical average velocity are less than 1% for all the elements used. This proves the accuracy of this type of mesh regardless of the number of elements. However, 204,000 elements are preferred due to the lower value of the relative error ($\varepsilon = 0.166$ and 0.146% for flow channels 11 and 12, respectively) and are used for the hydrodynamic analysis inside the CFSC reactor.

As illustrated in Figure 2, the velocity is not uniformly distributed in all parts of the CFSC reactor. Indeed, the velocity of the fluid is higher along the passage zone compared to the flow channel and the recirculation zone. This is due to the decrease in cross-sectional area along the passage zone of about 80 and 87.5% compared to that of the flow channel and the recirculation channel, respectively.

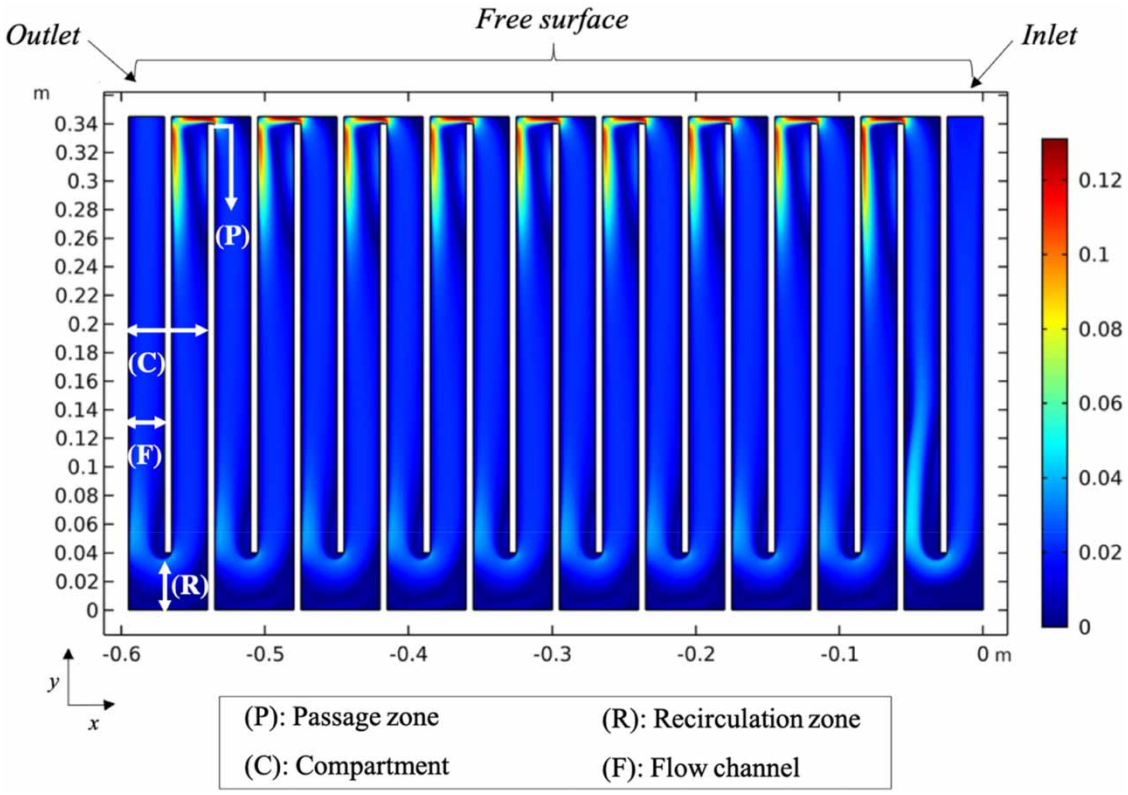

Figure 2 | Velocity field ($H_P = 0.5$ cm, $H_R = 4$ cm and $Q_V = 84.5\ \mathrm{L \cdot h^{-1}}$).

Furthermore, it is observed that the changes in flow directions generate the formation of a jet flow in the following flow channel. The magnitude of this jet flow is higher in the downflow channel at $0.26\ \mathrm{m} < y < 0.345\ \mathrm{m}$ because of the reduced cross-sectional area in the passage zone compared to the recirculation zone. However, regardless of its magnitude, the sudden change in flow direction greatly influences the velocity field in the CFSC reactor.

The streamlines in the x–y plane are presented in Figure 3; they indicate the flow behavior inside the CFSC reactor. In order to highlight the flow characteristics, three zooms are taken in three different locations in the CFSC reactor (passage zone, center of the flow channels, and recirculation zone) for two flow channels (channels 11 and 12 as shown in Figure 1).

As indicated in Figure 3, back mixing and recirculation of the flow occur on the opposite side of the flow channel following the passage zone or recirculation zone. In the upflow channel, back mixing and recirculation occur near the recirculation zone at y ranging from 0.04 to 0.07 m and occupy about 30–40% of the cross-sectional area of the upflow channel (Zoom (c)), while they occupy about 60% of the cross-sectional area of the downflow channel (Zoom (a)) at y ranging from 0.26 to 0.34 m, except for the second flow channel where the back mixing and recirculation range from 0.04 to 0.11 m. Finally, the flow tends to homogenize throughout the channel cross-section as it moves away from the passage and recirculation zones as shown in Figure 3 and zoom (b). Moreover, in the recirculation zone located at the bottom of the reactor, a dead zone is observed.

Figure 4 compares the obtained results from experimental tracing of the reactor using RTD methodology to that from numerical tracing using convection-diffusion equation. Globally, the profiles of the experimental and numerical $F(t)$ curves are approximately similar with a slight deviation. The first tracer concentration is observed, roughly, at the same time and the average residence time for numerical and experimental studies is 7 and 6.6 min, respectively, which corresponds to a difference of approximately 5%. Therefore, these similarities between numerical and experimental studies allow validating the results provided by CFD simulation of the hydrodynamic inside the CFSC reactor.

The main conclusion that emerges from the CFD simulation and the RTD study is that the velocity is not uniformly distributed inside the CFSC reactor. In the vicinity of the free surface, the streamwise velocity changes

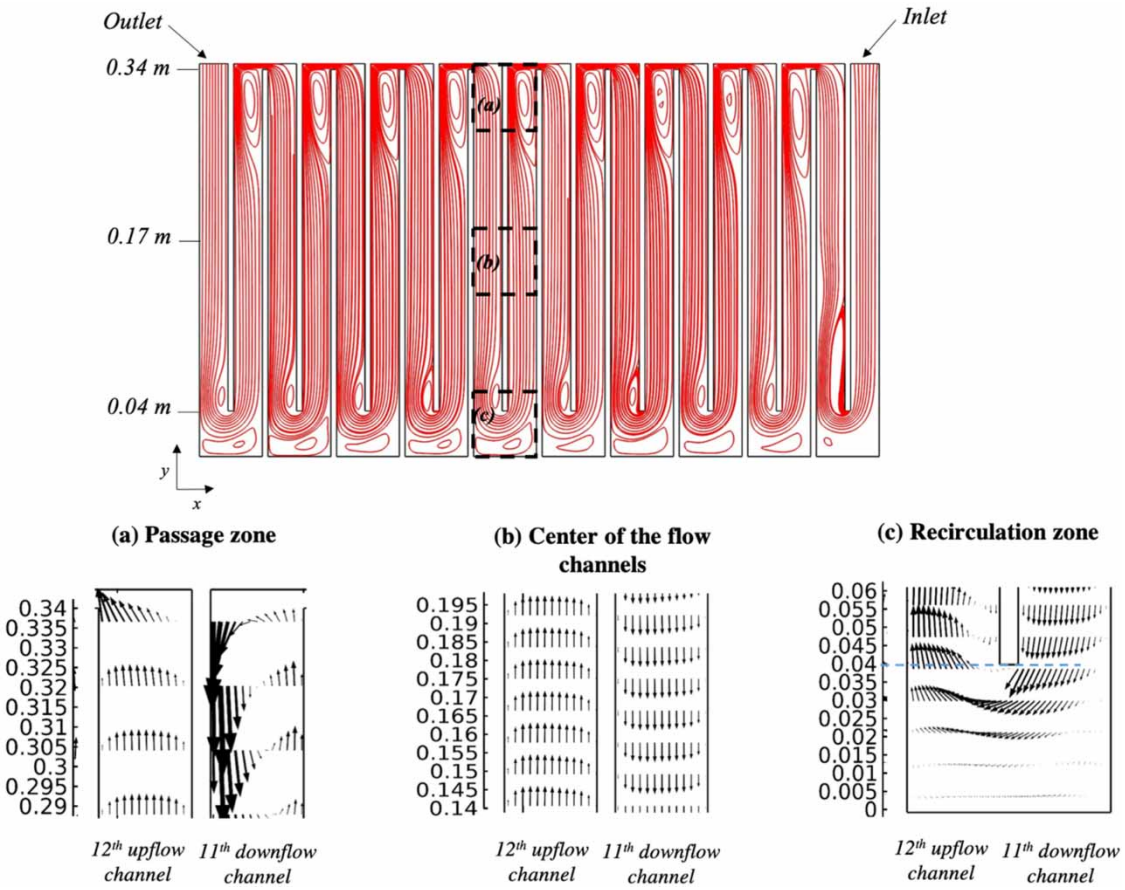

Figure 3 | Streamlines and velocity field inside the CFSC reactor.

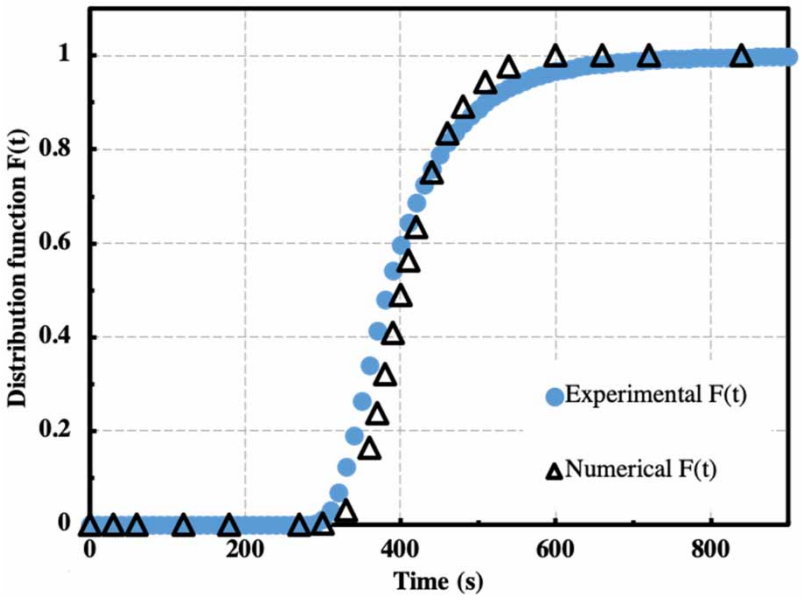

Figure 4 | Comparison between the distribution function obtained from numerical simulation and experimental data.

abruptly, and the local velocity of the liquid increases. Therefore, a large vortex is formed on top of the different downflow channels of the CFSC reactor as shown in Figure 3. The CFSC reactor can be used to perform further decolorization experiments, considering the stability of the flow in the reactor.

3.2. CFSC reactor performance for decolorization

The amount of electro-dissolved aluminum at the anode is strongly monitored by the applied current intensity and the electrolysis time. The electrochemical reactor of this study operated under current intensities ranging from 30 to 200 mA for investigating the decolorization of synthetic wastewater containing RR195 with an initial concentration of 10 mg · L^{-1}. These current intensity values are far lower than in conventional EC cells (Merzouk *et al.* 2009; Kobya *et al.* 2014; Assémian *et al.* 2018; Criado *et al.* 2020). Preliminary experiments were initiated to determine the range of current intensities under which high decolorization is reached, coagulant overdosage is avoided, and the useless high energy consumption is avoided. While applying current intensities ranging from 1 A to 200 mA to the EC reactor, the decolorization temporal evolution remained almost unchanged. Furthermore, at higher current intensities the resulting flocs are able to maintain their larger size due to the larger collision frequency owing to their high concentration (Harif & Adin 2011). All of this is a downside in our case since the flocs act as adsorbent and therefore a high specific surface area is required (Aoudj *et al.* 2010).

The flowrate was adjusted at 80 L · h^{-1} resulting in an average inlet velocity of 1.85 cm · s^{-1} (first downflow channel shown in Figure 1). On the free surface of the CFSC reactor, the flocs appear as a red colored layer which thickness depends largely on the current intensity and the electrolysis time. After about 60 min of operating under current intensities higher than 100 mA, the flocs floating on the free surface create a vertical thin gradient layer with the oldest flocs red on top and the youngest rather white at the bottom of the layer. This layering is a consequence of the decolorization temporal evolution, where the red layer comes from the reaction step as the treatment is still occurring, and the white layer is a result of the steady state during which the treatment remains unchanged regardless of the amount of the coagulant produced.

As might be expected, the flow visualization using the flocs formed during the electrochemical treatment confirms the numerical results shown in Figure 3. Experimentally, the jet flow formed in the passage zone and the increasing velocity carry away a part of the flocs formed at the free surface in the different channels of the CFSC reactor. However, the breakage of the flocs at the free surface only occurs when the flocs layer is thin enough. Conversely, a higher coagulant production leads to a highly stable thick flocs layer on the free surface withstanding the flow.

It is well established that the current intensity exhibits a much stronger influence on the kinetics of the decolorization than on its efficiency (Merzouk *et al.* 2009). This means that all current intensities are capable of yielding the same decolorization but at different electrolysis times. It is clear from Figure 5 that the increase of the current intensity from 100 to 200 mA does not allow an enhancement of the decolorization efficiency but rather causes the specific electrode consumption to increase remarkably as demonstrated in Figure 6.

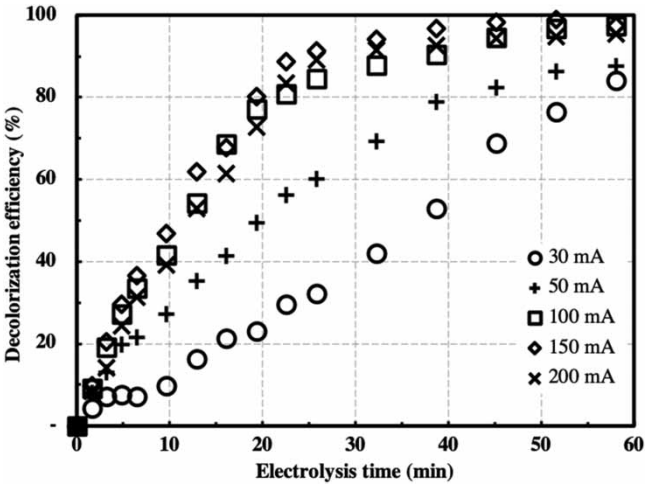

Figure 5 | Temporal evolution of decolorization efficiency for the different current intensities ($Q_v = 80$ L · h^{-1}, $C_0 = 10$ mg · L^{-1}, $\sigma_0 = 2,400$ μS · cm^{-1}).

Figure 5 reveals a similar decolorization efficiency evolution profile for all the higher current intensities. This profile follows two steps:

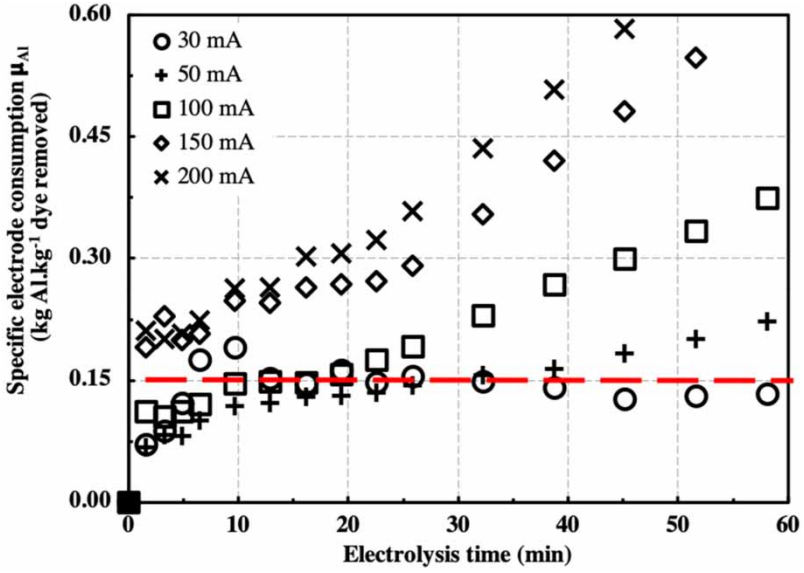

Figure 6 | Temporal evolution of specific electrode consumption for the different current intensities ($Q_v = 80\ L \cdot h^{-1}$, $C_0 = 10\ mg \cdot L^{-1}$, $\sigma_0 = 2,400\ \mu S \cdot cm^{-1}$).

- Reaction step: a sharp increase in the decolorization of synthetic wastewater appears. The treatment occurs rapidly owing to the availability of dye molecules. It is influenced by the current intensity; the higher the applied current the sharper the increase.
- Steady-state step: as the electrolysis time progresses, the rate of decolorization decreases. During this step, the decolorization of synthetic wastewater remains slightly unchanged. The residual amount of dye withstands the treatment despite the availability of the coagulant.

When the electrochemical reactor is operating under a current intensity of 30 mA, the decolorization efficiency evolution remains in the reaction step until the end of the experiment (Figure 5). At an electrolysis time of 58 min, the decolorization efficiency reached 80%. It might be explained by the insufficiency of the coagulant to uptake the dye molecules before that electrolysis time.

Conversely, when applying a current intensity of 50 mA, a decolorization efficiency of about 82% is obtained at a treatment time of approximately 45 min. However, when the reactor is operating under 100 and 150 mA, the electrolysis time yielding a decolorization efficiency of 80% is quasi-unchanged at about 20 min, while 200 mA requires only about 19 min to achieve the same decolorization efficiency as shown in Figure 5.

Figure 6 illustrates the temporal evolution of the specific electrode consumption for the different current intensities ranging from 30 to 200 mA.

As illustrated in Figure 6, the current intensities under 100 mA generate, at first, specific electrode consumptions under or equal to 0.15 kg $Al \cdot kg^{-1}$dye removed, while the current intensities above 100 mA generate specific electrode consumptions higher than 0.15 kg $Al \cdot kg^{-1}$ dye removed even before reaching the steady state. Nonetheless, reaching the steady-state condition leads to a linear relationship between the specific electrode consumption and the electrolysis time. This could be explained by Equation (3), when the steady state is established, the final dye concentration resists to the treatment. Thus, the decolorization efficiency remains almost unchanged. This leads to a specific electrode consumption that only changes as a function of the amount of the coagulant produced that is proportional to the current intensity applied and the electrolysis time (Equation (2)).

The slope of the linear region depends on the applied current intensity (Figure 6). This overconsumption of the electrodes is attributed to the over-production of the coagulant which is increased by raising the electrolysis time.

According to Merzouk *et al.* (2009), the specific electrode consumption is about 0.140 kg $Al \cdot kg^{-1}$ dye removed under an applied current intensity of 1.5 A and an initial concentration of 100 $mg \cdot L^{-1}$ of 2-naphthoic acid and 2-naphthol mixture for an 80% decolorization efficiency. Alternatively, Yuksel *et al.* (2012) reported the lowest electrode consumption for the removal of Reactive Yellow 135 from a real textile effluent at an initial dye concentration of 200 $mg \cdot L^{-1}$, being 0.153 kg $Al \cdot kg^{-1}$ dye removed under a current intensity of 143 mA to reach

40% of the decolorization efficiency. Therefore, in this study, 0.150 kg Al · kg^{-1} dye removed seems a reasonable limit value of the specific electrode consumption. This should be taken into consideration to preserve the electrodes' life span.

Table 2 displays the electrode consumption value at different electrolysis times for the different current intensities that yield a decolorization efficiency above 80%. At an electrolysis time of 26 min, increasing the applied current intensity from 100 to 200 mA only increases the decolorization efficiency by 7%, while the specific electrode consumption is raised by 46%.

Table 2 | Evolution of the decolorization efficiency above 80% with the corresponding specific electrode consumptions μ_{Al} (10^{-3} kg Al · kg^{-1} dye removed) for the different current intensities at different electrolysis times

	$I = 30$ mA		$I = 50$ mA		$I = 100$ mA		$I = 150$ mA		$I = 200$ mA	
Electrolysis time (min)	η (%)	μ_{Al}	η (%)	μ_{Al}	η (%)	μ_{Al}	η (%)	μ_{Al}	η (%)	μ_{Al}
19									80.11	312
26					84.57	195	89.20	296	91.40	364
32					87.77	234	91.48	361	94.09	443
39					90.43	273	92.61	428	96.77	516
45			82.39	187	94.68	304	94.32	490	98.39	593
52			86.36	204	96.81	340	94.89	557	97.85	674
58	84.15	135	87.50	226	97.34	381	95.45	623	97.31	771

The results in Table 2 confirm the previously discussed results in Figures 5 and 6. The rise of the applied current intensity from 30 to 100 mA results in an increase of the specific electrode consumption by 44% and a decrease of the electrolysis time by 55%. Moreover, increasing the current intensity from 50 to 100 mA decreases the electrolysis time by 42% and hardly raises the specific electrode consumption by 4%.

Hence, to reach a certain decolorization efficiency, a compromise between time and current intensity must be found. A high-current intensity provides a good decolorization efficiency in a short time, while a low-current intensity produces the same result over a longer time. As discussed, the increase of the current intensity generates many downsides such as overdosage of coagulant, excessive energy consumption, and electrodes' lifespan reduction; whereas a high electrolysis time allows good contact between the coagulant and dye molecules. However, when designing a reactor, a high time of treatment means larger equipment leading to large investment and operating costs.

The main conclusion that can be drawn from this part is that for an initial dye concentration of 10 mg · L^{-1}, the CFSC reactor operating in a closed-circuit and under steady-state conditions should be avoided to prevent useless energy consumption and overdosage of the coagulant. Considering that the transition from the reaction step to the steady state of decolorization efficiency of the current intensities (Figure 5) and the specific electrode consumption (Figure 6) occurs at about 26 min for a current intensity of 100 mA. The steady-state condition begins at this time. Hence, it will be referred to as the electrolysis time limit.

In reality, the inlet dye concentration of the textile wastewater plants might change. Thus, it is necessary to study the effects of this variation on the performance of the EC process. We have explored the specific electrode consumption and the decolorization efficiency for initial dye concentrations ranging from 5 to 50 mg · L^{-1} (Figure 7).

During the following experiments, the CFSC reactor operating in a closed-circuit (Figure 1) behaves more like a fed-batch system with the coagulant being added continuously. The feeding rate is monitored only by the current intensity as the electrolysis time is constant.

When the CFSC reactor is operating under a current intensity of 100 mA for an electrolysis time of 26 min, two distinct ranges of concentrations appear (Figure 7). First, when the initial dye concentration is between 5 and 10 mg · L^{-1}, a sharp decrease of the specific electrode consumption occurs while the decolorization efficiency is almost constant at about 0.15 kg Al · kg^{-1} dye removed. Second, the specific electrode consumption is quasi-constant, and the decolorization decreases almost linearly from 82 to 25% with increasing dye concentration from 10 to 50 mg · L^{-1}. This could be attributed to the adsorption capacity of the coagulant. At first, the

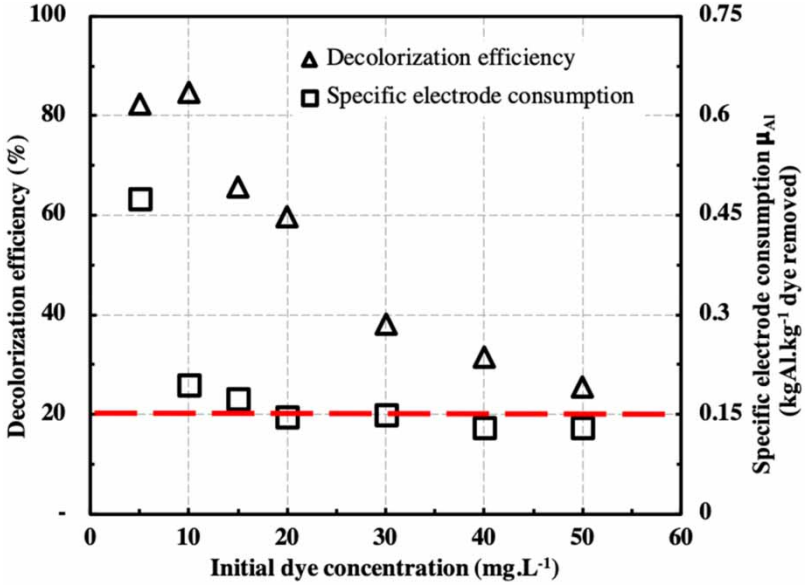

Figure 7 | Evolution of decolorization efficiency and specific electrode consumption as a function of the initial dye concentration ($Q_v = 80\ L \cdot h^{-1}$, $I = 100$ mA, $t = 26$ min, $\sigma_0 = 2, 400\ \mu S \cdot cm^{-1}$).

adsorption capacity is not yet exhausted due to the unavailability of the dye molecules, then it slowly stabilizes to reach exhaustion when there are surplus dye molecules in the solution. The coagulant adsorption capacity is exhausted when all the active sites are already occupied.

A robust process must be able to achieve the same decolorization efficiency regardless of the initial dye concentration value. In the following experiments, process performance was investigated, using various current intensities and initial dye concentrations (RR195), while maintaining the electrolysis time at 26 min, in order to estimate the current intensity yielding a decolorization of about 80% for each dye concentration.

The principal aim of these experiments is to create a resilient EC process that is capable of delivering satisfactory results even under critical conditions such as high initial dye concentrations.

Figure 8(a) shows that increasing the initial dye concentration decreases the decolorization efficiency for the same current intensity. The decolorization efficiency increases with increasing current intensity at a constant initial dye concentration. With the initial concentration value of 30 $mg \cdot L^{-1}$, the decolorization efficiency increased from 40 to 80% when the electrochemical reactor operated under 100 and 400 mA, respectively.

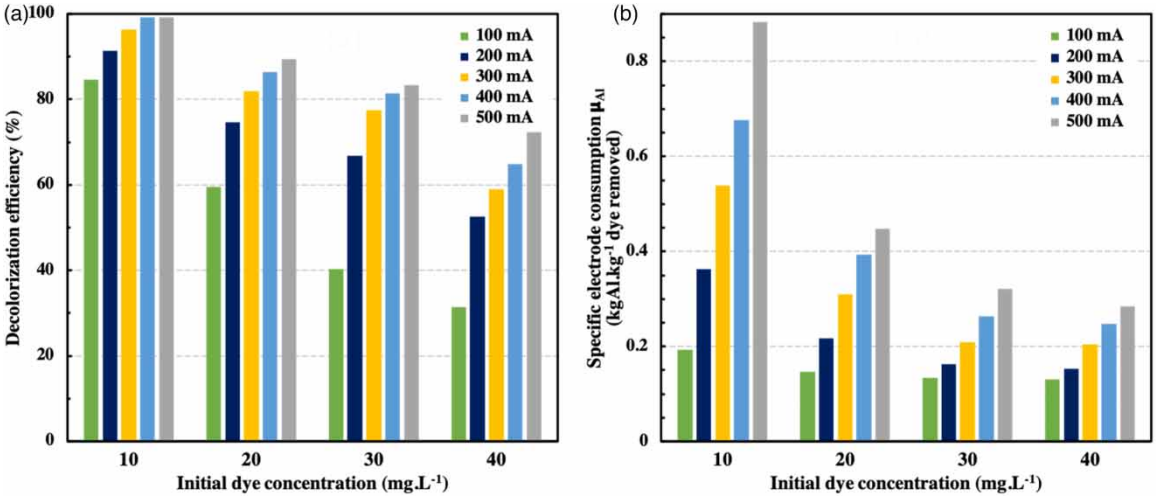

Figure 8 | Evolution of the decolorization efficiency and the specific electrode consumption as a function of the current intensity for the different initial dye concentrations ($Q_v = 80\ L \cdot h^{-1}$, $t = 26$ min, $\sigma_0 = 2, 400\ \mu S \cdot cm^{-1}$).

This is consistent with the theoretical background of the EC process according to which higher current intensities lead to increase dissolution of metal cations in the solution. Thus, as the amount of coagulant increases, the potential to adsorb dye molecules in solution also rises (Garcia-Segura *et al.* 2017). However, as illustrated in Figure 8(a), the rate of this process enhancement might change as a function of the initial dye concentration. For instance, at 10 $mg \cdot L^{-1}$, the decolorization efficiency increased only by 15% when the current intensity was raised from 100 to 500 mA; whereas for 40 $mg \cdot L^{-1}$, an increase of 41% under the same current intensities was recorded.

Specific electrode consumption was also evaluated for the CFSC reactor operating in a closed-circuit under different current intensities and initial dye concentrations and the same electrolysis time limit defined above as 26 min. As shown in Figure 8(b), an increase in the current intensity leads to a proportionate rise in the specific electrode consumption. For example, under the same current intensity of 500 mA, the respective electrode consumptions are about 0.88 kg $Al \cdot kg^{-1}$ dye removed and 0.28 kg $Al \cdot kg^{-1}$ dye removed for initial dye concentrations of 10 and 40 $mg \cdot L^{-1}$, respectively. However, at 500 mA the initial concentration of 10 $mg \cdot L^{-1}$ has already reached a decolorization efficiency of 99%. Therefore, the residual dye concentration in the solution is rather low to non-existent. In fact, the rate at which the specific electrode consumption increases with increasing current intensity is inversely proportional to raising the initial concentration.

Similar results were showcased by Chafi *et al.* (2011), using the EC process for the removal of Acid Orange 7. Increasing the initial dye concentration from 50 to 200 $mg \cdot L^{-1}$ leads to both a decrease of the decolorization efficiency from 90 to 75% and the specific electrode consumption from 2.2 kg $Al \cdot kg^{-1}$ dye removed to 0.7 kg $Al \cdot kg^{-1}$ dye removed.

Summing up, in the case of lower initial dye concentration, the decolorization efficiency is already at a maximum value. Therefore, the overdosage electro-dissolved aluminum is considered useless to the process. Conversely, higher initial dye concentration still provides significantly increasing decolorization efficiency with rising current intensity.

4. CONCLUSION

This integral study investigated the decolorization of synthetic wastewater containing Reactive Red 195 in a laboratory-scale EC process. A CFSC reactor operating in closed-circuit is chosen to keep the similar hydrodynamics of continuous mode. Besides the transfer phenomena study, this work described transport phenomena inside the reactor using CFD simulation and RTD methodology. Furthermore, the deployed approach takes into consideration mixing, decolorization efficiency, and specific electrode consumption.

CFD simulation results indicate that the velocity is not uniformly distributed in all parts of the CFSC reactor. At the passage zone located in the vicinity of the free surface, the streamwise velocity changes abruptly, and the local velocity of the liquid increases. This results in the formation of a large vortex on top of the different downflow channels of the CFSC reactor. While at the recirculation zone located at the bottom of the reactor, a dead zone is observed

The flow tends to homogenize throughout the channel cross-section as it moves away from the passage and recirculation zones. In general, considering the stability of the flow in the CFSC reactor, it can be used to perform further decolorization experiments.

For an initial dye concentration of 10 $mg \cdot L^{-1}$, the electrolysis time required to reach the steady-state conditions depends on the applied current intensity. However, our experimental data demonstrated that the temporal evolution of the decolorization remains unchanged when the current intensity exceeds 100 mA.

To achieve a decolorization efficiency of 80%, a decrease of about 40% in electrolysis time is observed when the electrochemical reactor operates under a current intensity of 100 mA instead of 50 mA. The deviation in the profile of the decolorization efficiency and the specific electrode consumption occurs at about 26 min, the steady-state condition begins at this treatment time, which is referred to as the electrolysis time limit. The electrolysis time limit is considered as an essential parameter for the transposition from closed-circuit to continuous mode.

When raising the initial dye concentration from 10 to 50 $mg \cdot L^{-1}$, the specific electrode consumption remained slightly unchanged at about 0.15 kg $Al \cdot kg^{-1}$ dye removed, meanwhile the decolorization efficiency demonstrated a remarkable decrease. Thus, for the same treatment time, the EC process could be enhanced by increasing the current intensity. This exploratory study using the CFSC reactor operating in closed-circuit to perform EC provides a solid base that might be useful for the transposition from batch to continuous mode.

ACKNOWLEDGEMENTS

The authors would like to thank Prof El Ibrizy Ouafa for providing linguistic advice and English proofing.

AUTHOR CONTRIBUTIONS

R.L. conceptualized and investigated the study, did software analysis, data curation, and formal analysis, prepared the methodology, wrote the original draft, wrote, reviewed, and edited the article. T.N.K. validated, visualized, wrote, reviewed, and edited the article. Z.Z. collected resources and did data curation. A.A. reviewed and edited the article. B.B. visualized, reviewed, and edited the article. K.D. collected resources and validated the study. A.D. conceptualized the study, did data curation, did project administration, supervised, wrote, reviewed and edited the article.

DATA AVAILABILITY STATEMENT

All relevant data are included in the paper or its Supplementary Information.

CONFLICT OF INTEREST

The authors declare there is no conflict.

REFERENCES

Ammayappan, L., Jose, S. & Raj, A. 2016 Sustainable production processes in textile dyeing. *Green Fashion: Environmental Footprints and Eco-Design of Products and Processes* (1), 185–216. https://doi.org/10.1007/978-981-10-0111-6_8.

Amour, A., Merzouk, B., Leclerc, J. P. & Lapicque, F. 2016 Removal of reactive textile dye from aqueous solutions by electrocoagulation in a continuous cell. *Desalin. Water Treat.* **57**(48–49), 22764–22773. https://doi.org/10.1080/19443994.2015.1106094.

Aoudj, S., Khelifa, A., Drouiche, N., Hecini, M. & Heamitouche, H. 2010 Electrocoagulation process applied to wastewater containing dyes from textile industry. *Chem. Eng. Process.* **49**(11), 1176–1182. https://doi.org/10.1016/j.cep.2010.08.019.

Ardhan, N., Ruttithiwapanich, T., Songkasiri, W. & Phalakornkule, C. 2015 Comparison of performance of continuous-flow and batch electrocoagulators: a case study for eliminating reactive blue 21 using iron electrodes. *Sep. Purif. Technol.* **146**, 75–84. https://doi.org/10.1016/j.seppur.2015.03.028.

Assémian, A. S., Kouassi, K. E., Drogui, P., Adouby, K. & Boa, D. 2018 Removal of a persistent dye in aqueous solutions by electrocoagulation process: modeling and optimization through Response Surface Methodology. *Water Air Soil Pollut.* **229**(6), 184. https://doi.org/10.1007/s11270-018-3813-2.

Attour, A., Touati, M., Tlili, M., Ben Amor, M., Lapicque, F. & Leclerc, J. P. 2014 Influence of operating parameters on phosphate removal from water by electrocoagulation using aluminum electrodes. *Sep. Purif. Technol.* **123**, 124–129. https://doi.org/10.1016/j.seppur.2013.12.030.

Benazzi, T. L., Di Luccio, M., Dallago, R. M., Steffens, J., Mores, R., Do Nascimento, M. S., Krebs, J. & Ceni, G. 2016 Continuous flow electrocoagulation in the treatment of wastewater from dairy industries. *Water Sci. Technol.* **73**(6), 1418–1425. https://doi.org/10.2166/wst.2015.620.

Bennajah, M., Gourich, B., Essadki, A. H., Vial, C. & Delmas, H. 2009 Defluoridation of Morocco drinking water by electrocoagulation/electroflottation in an Electrochemical external-loop airlift reactor. *Chem. Eng. J.* **148**(1), 122–131. http://dx.doi.org/10.1016/J.CEJ.2008.08.014.

Bidu, J. M., Van Der Bruggen, B., Rwiza, M. J. & Njau, K. N. 2021 Current status of textile wastewater management practices and effluent characteristics in Tanzania. *Water Sci. Technol.* **83**(10), 2363–2376. https://doi.org/10.2166/wst.2021.133.

Burkinshaw, S. M. & Salihu, G. 2018 The role of auxiliaries in the immersion dyeing of textile fibres: part 10 the influence of inorganic electrolyte on the wash-off of reactive dyes. *Dyes Pigm.* **149**, 652–661. https://doi.org/10.1016/j.dyepig.2017.11.034.

Cañizares, P., Carmona, M., Lobato, J., Martinez, F. & Rodrigo, M. A. 2005 Electrodissolution of Aluminum electrodes in electrocoagulation processes. *Ind. Eng. Chem. Res.* **44**(12), 4178–4185. https://doi.org/10.1021/ie048858a.

Chafi, M., Gourich, B., Essadki, A. H., Vial, C. & Fabregat, A. 2011 Comparison of electrocoagulation using iron and aluminium electrodes with chemical coagulation for the removal of a highly soluble acid dye. *Desalination* **281**, 285–292. https://doi.org/10.1016/j.desal.2011.08.004.

Choudhary, A. & Mathur, S. 2017 Performance evaluation of 3D rotating anode in electro coagulation reactor: part II: effect of rotation. *J. Water Process. Eng.* **19**, 352–362. https://doi.org/10.1016/j.jwpe.2017.08.019.

Criado, S. P., Gonçalves, M. J., Tavares, L. B. B. & Bertoli, S. L. 2020 Optimization of electrocoagulation process for disperse and reactive dyes using the response surface method with reuse application. *J. Cleaner Prod.* **275**, 122690. https://doi.org/10.1016/j.jclepro.2020.122690.

Dey, A. K. & Kumar, U. 2017 Adsorption of Reactive Red 195 from polluted water upon Na2CO3 modified jute fiber. *Int. J. Eng. Technol.* **9**(3S), 53–58. https://doi.org/10.21817/ijet/2017/v9i3/170903S011.

Doggaz, A., Attour, A., Mostefa, M. P., Côme, K., Tlili, M. & Lapicque, F. 2019 Removal of heavy metals by electrocoagulation from hydrogenocarbonate-containing waters: compared cases of divalent iron and zinc cations. *J. Water. Process. Eng.* **29**, 100796. https://doi.org/10.1016/j.jwpe.2019.100796.

Garcia-Segura, S., Eiband, M. M. S. G., Vieira de Melo, J. & Martinez-Huitle, C. A. 2017 Electrocoagulation and advanced electrocoagulation processes: a general review about the fundamentals, emerging applications and its association with other technologies. *J. Electroanal. Chem.* **801**, 267–299. https://doi.org/10.1016/j.jelechem.2017.07.047.

Graça, N. S., Ribeiro, A. M. & Rodrigues, A. E. 2019 Removal of Fluoride from water by a continuous electrocoagulation process. *Ind. Eng. Chem. Res.* **58**(13), 5314–5321. https://doi.org/10.1021/acs.iecr.9b00019.

Gündüz, Z. & Atabey, M. 2019 Effects of operational parameters on the decolourisation of Reactive Red 195 dye from aqueous solutions by electrochemical treatment. *Int. J. Electrochem. Sci.* **14**, 5868–5885. https://doi.org/10.20964/2019.06.37.

Hakizimana, J. N., Gourich, B., Chafi, M., Stiriba, Y., Vial, C., Drogui, P. & Naja, J. 2017 Electrocoagulation process in water treatment: a review of electrocoagulation modeling approaches. *Desalination* **404**, 1–21. https://doi.org/10.1016/j.desal.2016.10.011.

Harif, T. & Adin, A. 2011 Size and structure evolution of kaolin–Al(OH)3 flocs in the electroflocculation process: a study using static light scattering. *Water. Res.* **45**(18), 6195–6206. https://doi.org/10.1016/j.watres.2011.09.027.

Kobya, M., Gengec, E., Sensoy, M. T. & Demirbas, E. 2014 Treatment of textile dyeing wastewater by electrocoagulation using Fe and Al electrodes: optimisation of operating parameters using central composite design. *Color. Technol.* **130**(3), 226–235. https://doi.org/10.1111/cote.12090.

Mahanna, H. & Samy, M. 2020 Adsorption of Reactive Red 195 dye from industrial wastewater by dried soybean leaves modified with acetic acid. *Desalin. Water Treat.* **178**, 312–321. https://doi.org/10.5004/dwt.2020.24960.

McBeath, S. T., Nouri-Khorasani, A., Mohseni, M. & Wilkinson, D. P. 2020 *In-situ* determination of current density distribution and fluid modeling of an electrocoagulation process and its effects on natural organic matter removal for drinking water treatment. *Water. Res.* **171**, 115404. https://doi.org/10.1016/j.watres.2019.115404.

Merzouk, B., Gourich, B., Sekki, A., Madani, K., Vial, C. & Barkaoui, M. 2009 Studies on the decolorization of textile dye wastewater by continuous electrocoagulation process. *Chem. Eng. J.* **149**(1–3), 207–214. https://doi.org/10.1016/j.cej.2008.10.018.

Moussa, D. T., El-Naas, M. H., Nasser, M. & Al-Marri, M. J. 2017 A comprehensive review of electrocoagulation for water treatment: potentials and challenges. *J. Environ. Manage.* **186**, 24–41. https://doi.org/10.1016/j.jenvman.2016.10.032.

Munagapati, V. S., Wen, H., Gollakota, A. R. K., Wen, J., Lin, K. A., Shu, C., Reddy, G. M., Zyryanov, G. V., Wen, J. & Tian, Z. 2022 Removal of sulfonated azo Reactive Red 195 textile dye from liquid phase using surface-modified lychee (*Litchi chinensis*) peels with quaternary ammonium groups: adsorption performance, regeneration, and mechanism. *J. Mol. Liq.* **368**(A), 120657. https://doi.org/10.1016/j.molliq.2022.120657.

Nazari, P. & Setayesh, S. R. 2019 Effective degradation of reactive Red 195 via heterogeneous electro-Fenton treatment: theoretical study and optimization. *Int. J. Environ. Sci. Technol.* **16**(10), 6329–6346. https://doi.org/10.1007/s13762-018-2048-5.

Nie, X. & Li, L. 2015 A Comparison of low Reynolds number k – ε Models. In: *4th International Conference on Computer, Mechatronics, Control and Electronic Engineering (ICCMCEE)*. https://doi.org/ 10.2991/iccmcee-15.2015.250

Ntambwe Kambuyi, T., Eddaqaq, F., Driouich, A., Bejjany, B., Lekhlif, B., Mellouk, H., Digua, K. & Dani, A. 2019 Using Response Surface Methodology (RSM) for optimizing turbidity removal by electrocoagulation/electro-Flotation in an internal loop airlift reactor. *Water Supply* **19**(8), 2476–2484. https://doi.org/10.2166/ws.2019.129.

Ntambwe Kambuyi, T., Bejjany, B., Lekhlif, B., Mellouk, H., Digua, K. & Dani, A. 2021 Design of a continuous-flow single-channel reactor using optimal experimental data from batch reactor for turbidity removal by electrocoagulation. *J. Environ. Chem. Eng.* **9**(1), 104651. https://doi.org/10.1016/j.jece.2020.104651.

Pérez-Calderón, J., Santos, M. V. & Zaritzky, N. 2018 Reactive Red 195 dye removal using chitosan coacervated particles as bio-sorbent: analysis of kinetics, equilibrium and adsorption mechanisms. *J. Environ. Chem. Eng.* **6**(5), 6749–6760. https://doi.org/10.1016/j.jece.2018.10.039.

Rodrigues, A. A., Seki, C. C., Ramalho, L. S., Argondizo, A. & Silva, A. P. 2020 Electrocoagulation in fixed bed reactor – color removal in batch and continuous mode. *Sep. Purif. Technol.* **253**, 117481. https://doi.org/10.1016/j.seppur.2020.117481.

Samanta, K. K., Pandit, P., Samanta, P. & Basak, S. 2019 Water consumption in textile processing and sustainable approaches for its conservation. *Water in Textiles and Fashion: Consumption, Footprint, and Life Cycle Assessment* 41–59. https://doi.org/10.1016/C2017-0-03774-6

Somayajula, A., Asaithambi, P., Susree, M. & Matheswaran, M. 2012 Sonoelectrochemical oxidation for decolorization of Reactive Red 195. *Ultrason. Sonochem.* **19**(4), 803–811. https://doi.org/10.1016/j.ultsonch.2011.12.019.

Tegladza, I. D., Xu, Q., Xu, K., Lv, G. & Lu, J. 2021 Electrocoagulation processes: a general review about role of electro-generated flocs in pollutant removal. *Process Saf. Environ. Prot.* **146**, 169–189. https://doi.org/10.1016/j.psep.2020.08.048.

Thammachai, K. & Charoensuk, C. 2021 Coagulation of reactive red 195 dye by using polyaluminium chloride as coagulant. *AIP Conf. Proc.* **2396**, 030007. https://doi.org/10.1063/5.0066312.

Umadevi, M., Rathinam, R., Brindha, T., Dheenadhayalan, S. & Pattabhi, S. 2022 Application of electro- chemical oxidation for the treatment of reactive red 195 using graphite electrode. *Asian. J. Biol. Life. Sci.* (10), 620–625. https://doi.org/ 10.5530/ajbls.2021.10.82.

Villalobos-Lara, A. D., Pérez, T., Uribe, A. R., Alfardo-Ayala, A., Jesùs Ramírez-Minguela, J. & Minchaca-Mojica, I. J. 2020 CFD simulation of biphasic flow, mass transport and current distribution in a continuous rotating cylinder electrode reactor for electrocoagulation process. *J. Electroanal. Chem.* **858**, 113807. https://doi.org/10.1016/j.jelechem.2019.113807.

Yang, S., Sun, J., Wu, K. & Hu, C. 2021 Enhanced oil droplet aggregation and demulsification by increasing electric field in electrocoagulation. *Chemosphere* **283**, 131123. https://doi.org/10.1016/j.chemosphere.2021.131123.

Yuksel, E., Gurbulak, E. & Eyvaz, M. 2012 Decolorization of a reactive dye solution and treatment of a textile wastewater by electrocoagulation and chemical coagulation: Techno-Economic comparison. *Environ. Prog. Sustainable Energy* **31**(4), 524–535. https://doi.org/10.1002/ep.10574.

Zheng, J., Zhao, R., Uliana, A. A., Liu, Y., Donnea, D., Zhang, X., Xu, D., Gao, Q., Jin, Y., Volodine, A., Zhu, J. & Van der Bruggen, B. 2022 Separation of textile wastewater using a highly permeable resveratrol-based loose nanofiltration membrane with excellent anti-fouling performance. *Chem. Eng. J.* **434**, 134705. https://doi.org/10.1016/j.cej.2022.134705.

First received 9 November 2022; accepted in revised form 20 April 2023. Available online 4 May 2023